High-Pressure Phase Transitions and Mechanisms in Lanthanum Mononitride

Hao Chen(陈昊)[1], Dan Zhou(周丹)[1*], Ying Xu(徐瑛)[1], and Quan Li(李全)[2*]

[1]*School of Physics, Changchun University of Science and Technology, Changchun 130022, China*
[2]*State Key Lab of Superhard Materials and Key Laboratory of Material Simulation Methods & Software of Ministry of Education, College of Physics, Jilin University, Changchun 130012, China*

(Received 2 April 2025; accepted manuscript online 22 April 2025)

A longstanding discrepancy between theoretical predictions and experimental observations on the high-pressure structural transformations of lanthanum mononitride (LaN) has posed challenges for understanding the behavior of heavy transition metal mononitrides. Here, we systematically investigate the structural evolution of LaN under high pressure using first-principles calculations combined with angle-dispersive synchrotron X-ray diffraction, identifying the phase transition sequence and corresponding phase boundaries. Analyses of energetics, kinetic barriers, and lattice dynamics reveal distinct mechanisms driving these transitions. These results clarify the structural stability of LaN and offer guidance for studying other heavy transition metal mononitrides with complex electronic behavior under extreme conditions.

DOI: 10.1088/0256-307X/42/6/067301 CSTR: 32039.14.0256-307X.42.6.067301

1. Introduction. The lanthanide series, consisting of elements with atomic numbers 57–71, from lanthanum (La) to lutetium (Lu), has received considerable attention for their applications in advanced materials.[1–4] As the atomic number increases within the series, the 4f orbitals become progressively filled. Chemically, lanthanides exhibit remarkable similarity due to their shared characteristics, with only gradual variations, stemming from the fact that distinctive 4f electron configurations are typically not participating in chemical bonding.[5]

Lanthanide mononitrides exhibit exceptional mechanical, electrical, optical, magnetic, and catalytic properties, which are highly sensitive to variations in external pressure and temperature conditions.[6–13] However, determining the crystal symmetry and atomic arrangements of lanthanide mononitrides from experimental X-ray diffraction (XRD) patterns is often challenging due to the weak scattering cross-section of nitrogen atoms. To address these complexities, several effective theoretical methods for structural predictions have been employed,[14–17] enabling the resolution of complex phases under extreme conditions. Nevertheless, the presence of inevitable kinetic barriers between the high-pressure thermodynamic phases can result in the hysteresis effect and structural coexistence, complicating the phase transition sequence.[18–23] Consequently, the structural evolution and phase transition mechanisms of lanthanide mononitrides remain subjects of ongoing debate.

As the first element in the lanthanide series, La possesses the simplest electronic structure within the group due to the absence of 4f electrons. This unique characteristic simplifies its electronic properties and makes La an ideal model system for investigating the phase transition behaviors of lanthanide mononitrides under high-pressure conditions.

To investigate the high-pressure phase transitions and their underlying mechanisms, we have selected lanthanum mononitrides (LaN) as representative materials for this study. At ambient conditions, LaN adopts a NaCl-type ($Fm\bar{3}m$) structure as its ground state.[24] However, this phase is dynamically unstable at low temperatures,[25] transitioning to an $Imm2$ phase via symmetry breaking.[26] Under compression, LaN has been theoretically predicted to undergo a phase transition from $Fm\bar{3}m$ to $Pm\bar{3}m$ across a broad and inconsistent pressure range of 25.3 to 169.0 GPa.[27–31] Experimentally, only a $P4/nmm$ phase has been reported to be synthesized at 22.8 GPa by angle-dispersive synchrotron XRD measurement.[32] There has also been speculation regarding the potential existence of a NiAs-type structure, analogous to the high-pressure polycrystalline BaO, although this phase has not yet been experimentally observed.[32]

Recent calculations suggest that the $P4/nmm$ structure is dynamically unstable up to 70 GPa,[33] prompting the search for more stable alternatives. The recently performed structural prediction has proposed additional candidate phases, including an anti-ferroelectric orthorhombic $Pbcm$ phase at about 20 GPa and a hexagonal $P6_3/mmc$ phase at about 10 GPa, resembling the NiAs-type structure in BaO.[33] However, the $P6_3/mmc$ phase is dynamically unstable at 0 K. Further structural optimizations have led to the discovery of a novel $P6_3mc$ structure, which lacks spatial inversion symmetry and demonstrates dynamic stability.[33] These newly predicted structures exhibit notable energy favorability over the $P4/nmm$ phase.

Despite these theoretical advances, experimental vali-

*Corresponding authors. Email: zhoudan@cust.edu.cn; liquan777@jlu.edu.cn

dation of these predicted phases remains limited. Moreover, inconsistencies between theoretical predictions and experimental observations persist, particularly regarding the sequence and stability of high-pressure phases. A systematic and comprehensive investigation is thus required to resolve these discrepancies and establish a consistent understanding of their structural evolution under high pressure.

In this study, we combined synchrotron angle-dispersive XRD experiments with first-principles calculations to resolve the long-standing controversy over the high-pressure phase transition sequence of LaN. By systematically analyzing the experimental XRD data alongside calculated enthalpies, transition barriers, and phonon dispersion, we identified three distinct phases of $Fm\bar{3}m$, $P6_3mc$, and $Pbcm$ structures that emerge sequentially with increasing pressure. This comprehensive investigation clarifies the structural evolution of LaN and offers a framework for exploring analogous phase transitions in other lanthanide mononitrides.

2. Method. High-pressure angle-dispersive XRD experiments were conducted at room temperature using a synchrotron X-ray source ($\lambda = 0.4859$ Å) at the B2 High-Pressure Station of the Cornell High Energy Synchrotron Source. A Mao-Bell-type diamond anvil cell equipped with 400 µm culet diamond anvils was utilized to pre-indent a T-301 stainless steel gasket to a central thickness of 50 µm. A 120 µm diameter hole was drilled at the center of the gasket to create the sample chamber. Commercially available LaN powder (Alfa Products, 99.999% purity) was loaded into the chamber with silicone oil serving as the pressure-transmitting medium. Pressure was determined based on the frequency shift of the ruby R1 fluorescence line.[34] Diffraction patterns were recorded using a MAR165 image plate, with an average acquisition time of 300 s. The two-dimensional XRD diffraction images were integrated using FIT2D software, which produces patterns of intensity versus diffraction angle 2θ.[35,36] Rietveld profile matching and refinement were performed using the GSAS+EXPGUI programs.[37,38] First-principles calculations were performed within the framework of density functional theory using the Vienna *ab initio* simulation package (VASP).[39,40] The Perdew–Burke–Ernzerhof functional within the generalized gradient approximation was employed to describe electron exchange-correlation effects.[41] The projector-augmented wave method was employed to treat the electron–ion interaction with the $5s^2 5p^6 5d^1 6s^2$ and $2s^2 2p^3$ configured as the valence electrons for La and N atoms, respectively. A plane-wave energy cutoff of 700 eV was adopted for all calculations. The geometry optimization and atomic relaxation were conducted using the conjugate gradient algorithm, with convergence thresholds set to 1×10^{-6} eV/atom for energy and 1×10^{-3} eV/Å for residual forces. Brillouin zone sampling was performed using the Monkhorst-Pack scheme with a grid spacing of $2\pi \times 0.02$ Å^{-1}. Structural predictions for LaN were performed using the CALYPSO crystal structure analysis method based on particle swarm optimization in the 0–100 GPa range.[12,42] Each structural search was performed with a population size of 20 and evolved over 20–40 generations. In each generation, 60% of the candidate structures were generated using the discrete particle swarm optimization method. Enthalpy was employed as the fitness function to guide the search toward thermodynamically favorable configurations. Lattice matching of initial and final phase transition structures was performed using the CSM (crystal-structure matches) method, accommodating up to 8 supercells.[43] The generalized solid-state nudged elastic band (G-SSNEB) method was applied to compute the transition states between initial and final structures.[44,45] Phonon dispersion relations were computed using the finite displacement method implemented in the PHONOPY package. Supercell sizes of $4\times4\times4$ (128 atoms), $3\times3\times3$ (108 atoms), $3\times3\times3$ (108 atoms), and $4\times2\times2$ (128 atoms) were employed for phases of $Fm\bar{3}m$, $Imm2$, $P6_3/mc$, and $Pbcm$, respectively.[46] The *ab initio* molecular dynamics (AIMD) simulations were performed under the NVT ensemble and combined with temperature-dependent effective potentials (TDEP)[47] were employed to assess dynamic stability in a $4\times4\times4$ (128 atoms) supercell for 12 ps with a timestep of 1.0 fs at 300 K.

3. Results and Discussion. We performed a comprehensive structural search for LaN under high-pressure conditions, utilizing the CALYPSO method in conjunction with first-principles calculation. This approach enables the prediction of thermodynamically stable and metastable structures based solely on the chemical composition, and its significant reliability and efficiency have been well established in previous studies.[48–55] At 0 K and 0 GPa, the $Imm2$ phase is found to be more stable than the conventional $Fm\bar{3}m$ phase, with a lower enthalpy of 14.6 meV as shown in Fig. 1. As pressure increases, LaN undergoes a sequence of phase transitions. The first transition occurs at 11.0 GPa from the $Imm2$ phase to the

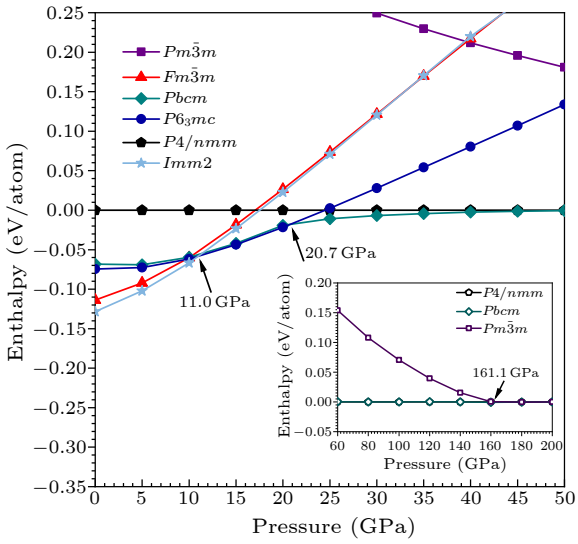

Fig. 1. Calculated enthalpy differences of the $Fm\bar{3}m$, $Imm2$, $P6_3mc$, $Pbcm$, and $Pm\bar{3}m$ phases of LaN relative to the $P4/nmm$ phase as a function of pressure, based on first-principles calculations at 0 K. The inset shows a focused comparison of the enthalpy differences for the $Pbcm$ and $Pm\bar{3}m$ phases, also referenced to the $P4/nmm$ phase, emphasizing their near-degenerate stability at high pressures.

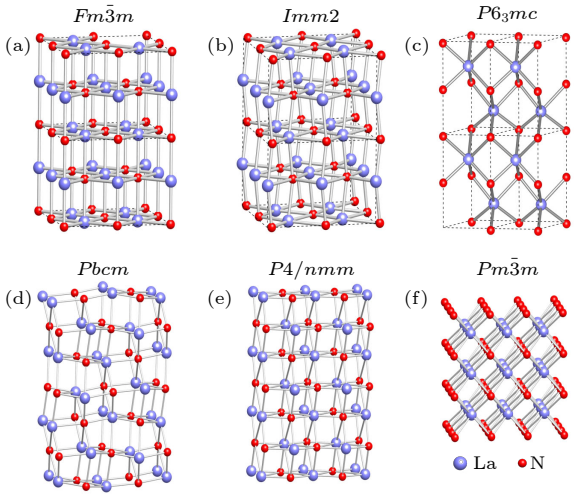

Fig. 2. The structural diagrams of identified phases of the (a) $Fm\bar{3}m$, (b) $Imm2$, (c) $P6_3mc$, (d) $Pbcm$, (e) $P4/nmm$, and (f) $Pm\bar{3}m$ structures.

$P6_3mc$ phase, followed by a second transition to the orthorhombic $Pbcm$ phase at 20.7 GPa (see Fig. 1). Above 50 GPa, the enthalpy difference between the $P4/nmm$ and the $Pbcm$ structures becomes negligible as shown in Fig. 1. The transition to the $Pm\bar{3}m$ phase appears only at very high pressures, around 161.1 GPa shown in the inset of Fig. 1, emphasizing the complex and multi-stage phase transition behavior of LaN under extreme conditions. These findings are in close agreement with the previously theoretical studies,[26,33] providing further validation for the proposed phase transition sequence. To provide a clear and comprehensive view of the structural evolution of LaN under varying pressure conditions, the crystal structures of these phases, along with their respective lattice parameters and Wyckoff positions, are presented in Figs. 2(a)–2(f) and summarized in Table 1.

To assess the dynamical stability of LaN, we performed phonon dispersion calculations for each phase within their respective stable pressure ranges [Figs. 3(a)–3(d)]. The absence of imaginary frequencies in the phonon dispersion for the $Imm2$, $P6_3mc$, and $Pbcm$ phases confirms that these phases remain dynamically stable with respect to small perturbations and maintain their structural integrity under the applied compressive conditions. In contrast, the $Fm\bar{3}m$ structure, which is traditionally regarded as stable under ambient conditions, exhibits significant imaginary frequencies at high-symmetry points, specifically at M (0.5, 0, 0.5) and Γ (0, 0, 0). This dynamical instability provides valuable insight into the phase transition process at various temperature and pressure conditions for LaN. To further explore this behavior, we employed the TDEP method combined with AIMD simulations to calculate the phonon dispersion at 300 K.[47]

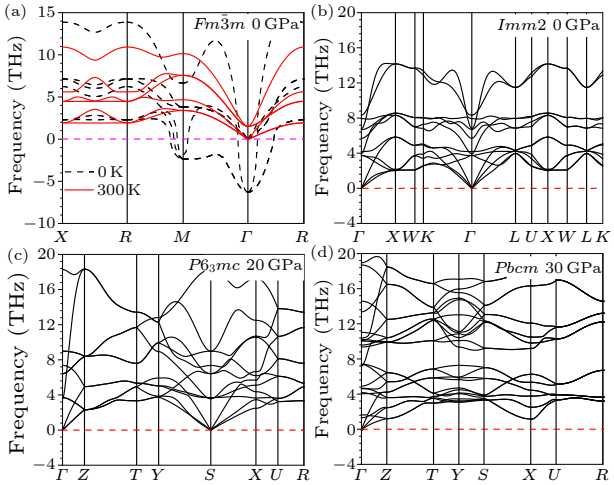

Fig. 3. Phonon dispersion curves of LaN for various structural phases under selected pressure conditions. (a) The $Fm\bar{3}m$ phase at 0 GPa, where the dashed lines represent calculations at 0 K and solid lines correspond to results at 300 K obtained via the TDEP method, showing temperature-induced dynamical stabilization. (b) The $Imm2$ phase at 0 GPa, exhibiting no imaginary frequencies and indicating dynamical stability at ambient conditions. (c) The $P6_3mc$ phase at 20 GPa. (d) The $Pbcm$ phase at 30 GPa. Both (c) and (d) also show dynamically stable phonon modes.

Table 1. The lattice parameters and Wyckoff positions for the $Fm\bar{3}m$ phase at 1.2 GPa, $Imm2$ phase at 0 GPa, $P6_3mc$ phase at 19.8 GPa, $Pbcm$ phase at 32.3 GPa, $P4/nmm$ phase at 60.0 GPa, and $Pm\bar{3}m$ phase at 161.1 GPa, respectively.

	Theory			Experiments
Phase	Lattice constants (Å)	Atom	Wyckoff positions	Lattice constants (Å)
$Fm\bar{3}m$	$a = 5.286$	La	4a (0.500, 0.500, 0.500)	$a = 5.269$
		N	4b (0.000, 0.000, 0.000)	
$Imm2$	$a = 5.175$	La	2a (0.500, 0.500, 0.482)	
	$b = 3.818$	N	2c (0.000, 0.000, 0.900)	
	$c = 3.817$			
$P6_3mc$	$a = 3.442$	La	2b (0.333, 0.667, 0.216)	$a = 3.442$
	$c = 6.124$	N	2a (0.000, 0.000, 0.000)	$c = 6.132$
$Pbcm$	$a = 3.194$	La	4d (0.832, 0.035, 0.250)	$a = 3.192$
	$b = 5.948$	N	4c (0.556, 0.075, 0.500)	$b = 5.953$
	$c = 5.910$			$c = 5.884$
$P4/nmm$	$a = 4.062$	La	2c (0.500, 0.000, 0.858)	
	$c = 3.028$	N	2b (0.500, 0.500, 0.500)	
$Pm\bar{3}m$	$a = 2.694$	La	1a (0.000, 0.000, 0.000)	
		N	1b (0.500, 0.500, 0.500)	

These simulations, which are essential for exploring the temperature effects on phonon behavior, revealed the absence of imaginary frequencies at both the M and Γ points in the $Fm\bar{3}m$ structure at elevated temperatures. The current results indicate that the $Fm\bar{3}m$ phase exhibits dynamic stability under thermal conditions, which validates previous research suggesting the potential stability of the $Fm\bar{3}m$ phase at higher temperatures.[26] Our findings provide evidence for the potential temperature-induced structural transformation from the $Imm2$ phase to the $Fm\bar{3}m$ phase in LaN, emphasizing the importance of thermal effects in driving phase transitions. This structural transformation could be accompanied by a symmetry-breaking mechanism, particularly under high-temperature conditions. This insight may have broader implications for understanding the behavior of other materials with NaCl-type crystal prototypes, such as SnTe, where thermal effects could play a significant role in symmetry-breaking transitions.[19]

To validate the theoretical predictions, angle-dispersive synchrotron XRD experiments were conducted under high-pressure conditions. The XRD patterns of LaN up to 40.6 GPa are shown in Fig. 4. A new diffraction peak at 10.4° appeared distinctly at 19.8 GPa, marking the onset of an intermediate phase. As pressure increases to 23.3 GPa, this peak becomes more pronounced, while the peaks at 9.5°, 11.0°, and 15.5° diminish in intensity, and a new peak at 9.2° emerges. The peak at 10.4° also began to broaden, indicating the transition from the intermediate phase to the high-pressure phase at 23.3 GPa. After reaching 32.3 GPa, the XRD patterns showed no further prominent changes, which suggests the phase transition was complete. Our experimental XRD measurements demonstrate that upon rapid decompression, the diffraction pattern of LaN reverts to that of the original structure, indicating that the high pressure-induced phase transitions are reversible. This observation suggests that, despite the presence of kinetic barriers during compression, the energy landscape permits the system to return to its initial phase once the pressure is released. The reversibility of the transition also implies that no irreversible structural reconstruction or chemical reaction occurs under the pressure conditions employed.

To determine the crystal structure of LaN, we refined the experimental patterns and simulated the XRD results

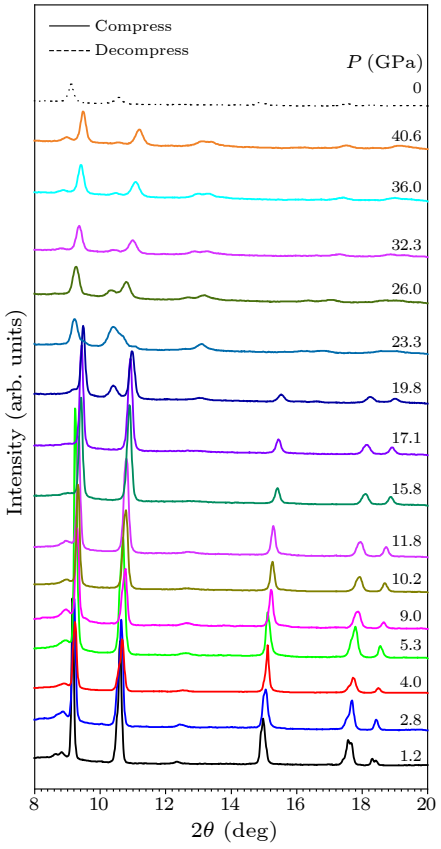

Fig. 4. The XRD patterns of LaN collected during compression and subsequent decompression (from bottom to top). With increasing pressure, new diffraction peaks emerge, indicating phase transitions from the initial $Fm\bar{3}m$ structure to intermediate and high-pressure phases. Upon decompression to ambient pressure, the diffraction pattern reverts to that of the initial phase, suggesting that the structural transitions are reversible. All measurements were performed using synchrotron radiation with a wavelength of $\lambda = 0.4859$ Å.

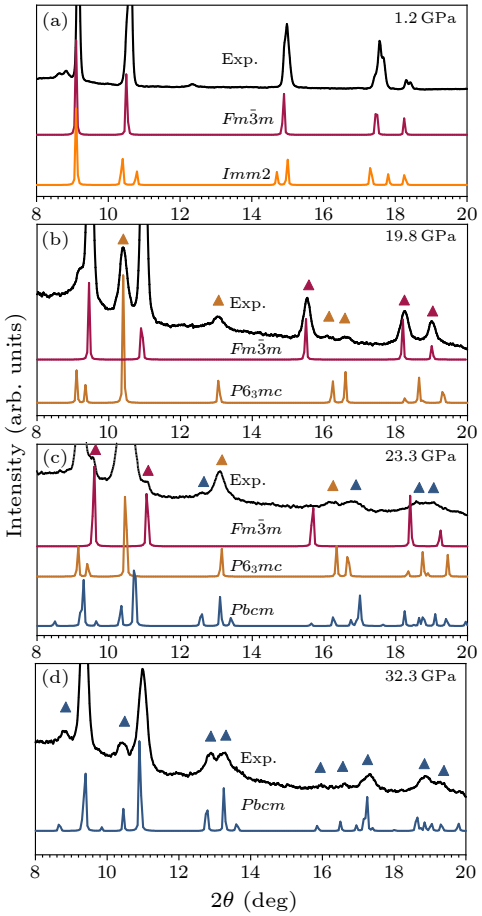

Fig. 5. Comparison of experimental and simulated XRD patterns at selected pressures: (a) 1.2 GPa, showing the $Fm\bar{3}m$ phase; (b) 19.8 GPa, corresponding to the emergence of the intermediate $P6_3mc$ phase; (c) 23.3 GPa, indicating the coexistence of the $P6_3mc$ and the $Pbcm$ phases; and (d) 32.3 GPa, where the high-pressure $Pbcm$ phase becomes dominant. The good agreement between simulation and experiment supports the proposed phase transition sequence.

based on the predicted structures, as shown in Figs. 5(a)–5(d). At 1.2 GPa [Fig. 5(a)], the $Fm\bar{3}m$ phase closely correlates with the experimental XRD diffraction pattern. In contrast, the $Imm2$ structure, while sharing a primary peak at 9.1° and 18.2° like the $Fm\bar{3}m$ phase, exhibits additional split peaks at 10.4°, 10.8°, 14.7°, 15.0°, 17.3°, and 17.8°, respectively. The $Fm\bar{3}m$ phase, representing a face-centered cubic structure, maintains high symmetry, whereas the $Imm2$ phase results from a symmetry reduction, leading to more diffraction peaks. This broken symmetry is a crucial factor contributing to the observed differences in the diffraction pattern. At a pressure of 19.8 GPa [Fig. 5(b)], the peak at 10.4° in the experimental data matches the diffraction pattern characteristic of the $P6_3mc$ phase, confirming it as an intermediate phase in the LaN transition. At 23.3 GPa [Fig. 5(c)], a new peak at 12.6° marks the initiation of high-pressure phase formation. Additionally, the presence of peaks at 9.6°, 10.5°, 11.1°, 13.1°, 16.3°, and 18.8° indicates that both the low-pressure and intermediate phases coexist within the system at this pressure. These observations highlight the presence of phase coexistence under these conditions. As the pressure increases to 32.3 GPa [Fig. 5(d)], the peaks at 8.8°, 10.5°, 12.9°, 13.3°, and 17.3° intensify, signifying that the system is predominantly characterized by the $Pbcm$ phase. At this stage, the low-pressure and intermediate phases completely disappear, marking the completion of the phase transition. Our experimental findings demonstrate that LaN undergoes a phase transition sequence under high pressure, transitioning from $Fm\bar{3}m$ to $P6_3mc$, and then to $Pbcm$, with phase transition points observed at 19.8 GPa and 23.3 GPa, respectively. The experimental lattice parameters for the $Fm\bar{3}m$, $P6_3mc$, and $Pbcm$ phases at 1.2 GPa, 19.8 GPa, and 32.3 GPa are listed in Table 1, in good agreement with our theoretical results.

After determining the sequence of phase transitions of LaN under high pressure, we further investigated the underlying mechanisms driving each transition. Kinetic barriers and thermodynamic energetics describe two fundamentally different aspects of phase transitions or chemical transformations. Kinetic barriers determine the rate and feasibility of a phase transition, while thermodynamic energetics dictate whether the transition is energetically favorable. To this end, we employed the G-SSNEB calculations to analyze the enthalpy barriers associated with these phase transitions. This method can be used to study phase transformations, in which cell degrees of freedom and not just internal degrees of freedom are necessary. For example, martensitic transformation is the most distinctive type of solid-state transformation among various types; the G-SSNEB method has revealed new insights into the intricate mechanisms governing this transformation.[44,45,56] Initially, the CSM method was used to match the structural characteristics of the initial and final states, ensuring that the transition pathways were properly mapped. Such a description fully exploits the translational and rotational symmetries and is independent of the choice of supercells.[43] To optimize the matching process, we utilized a maximum of 8 supercells, which led to the discovery of over 12000 potential matching patterns. From this large pool, the most plausible structures were selected for further G-SSNEB calculations. The results are presented in Figs. 6(a)–6(c).

We first investigated the enthalpy barrier associated with the transformation from the $Fm\bar{3}m$ phase to the $Imm2$ phase at 0 GPa [Fig. 6(a)]. Our findings revealed that the enthalpy difference between these two phases is minimal, with an enthalpy difference of only 14.6 meV. Interestingly, there is no enthalpy barrier between the two structures. This suggests that the $Fm\bar{3}m$ phase can transition spontaneously to the $Imm2$ phase at low temperature and ambient pressure conditions. The absent enthalpy barrier between these two phases implies that the transition is energetically favorable, which can occur without the need for external perturbation. Subsequently, we explored the enthalpy barriers for the transition from the $Imm2$ to the $P6_3mc$ phase at pressures of 11.0, 15.0, and 19.8 GPa [Fig. 6(b)]. At 11.0 GPa, we observed a relatively high enthalpy barrier of 70.6 meV. The enthalpy barrier from the $Imm2$ to the $P6_3mc$ phase shows minimal variation with increasing pressure. Although thermodynamic stability is typically evaluated based on enthalpy differences between competing phases, the actual occurrence of a phase transition is also governed by the kinetic barrier that must be overcome along the transition pathway. In the current case of LaN, while the $Imm2$ to the $P6_3mc$ transition is thermodynamically favorable at elevated pressures, the relatively high enthalpy barrier ($\sim$ 70.6 meV at 11.0 GPa) hinders the transformation, resulting in a delayed phase transition and hysteresis as observed in our experiments. By elucidating the underlying enthalpy barriers and structural transformations, it highlights the intricate mechanisms that govern the delayed response of the material to changing external pressure conditions. This analysis offers a detailed atomic-scale explanation for the hysteresis effect observed during the phase transition process, which may be observed in a wider variety of materials.[19]

Then we investigated the enthalpy barriers for the transition from the $P6_3mc$ to the $Pbcm$ structure [Fig. 6(c)]. Here, the results revealed remarkably low enthalpy barriers, with values of less than 1.0 meV at pressures of 20.7 GPa, 22.0 GPa, and 23.3 GPa. These results indicate that the transition between the $P6_3mc$ and the $Pbcm$ phases is highly favorable at these pressures, with the transition being nearly thermodynamically instantaneous under these conditions. This is in line with our experimental studies suggesting that the $P6_3mc$ phase can indeed be easily synthesized from the $Pbcm$ structure and further supports the notion that phase transitions between these two phases occur with minimal energetic cost. Figures 6(d)–6(f) illustrate the three distinct phase transition pathways observed during the G-SSNEB calculations.[44,45] These findings align with our enthalpy barrier analysis, where a significant enthalpy barrier of 70.6 meV is observed for the transition from the $P6_3mc$ phase to the $Pbcm$ phase, signifying a more complex and

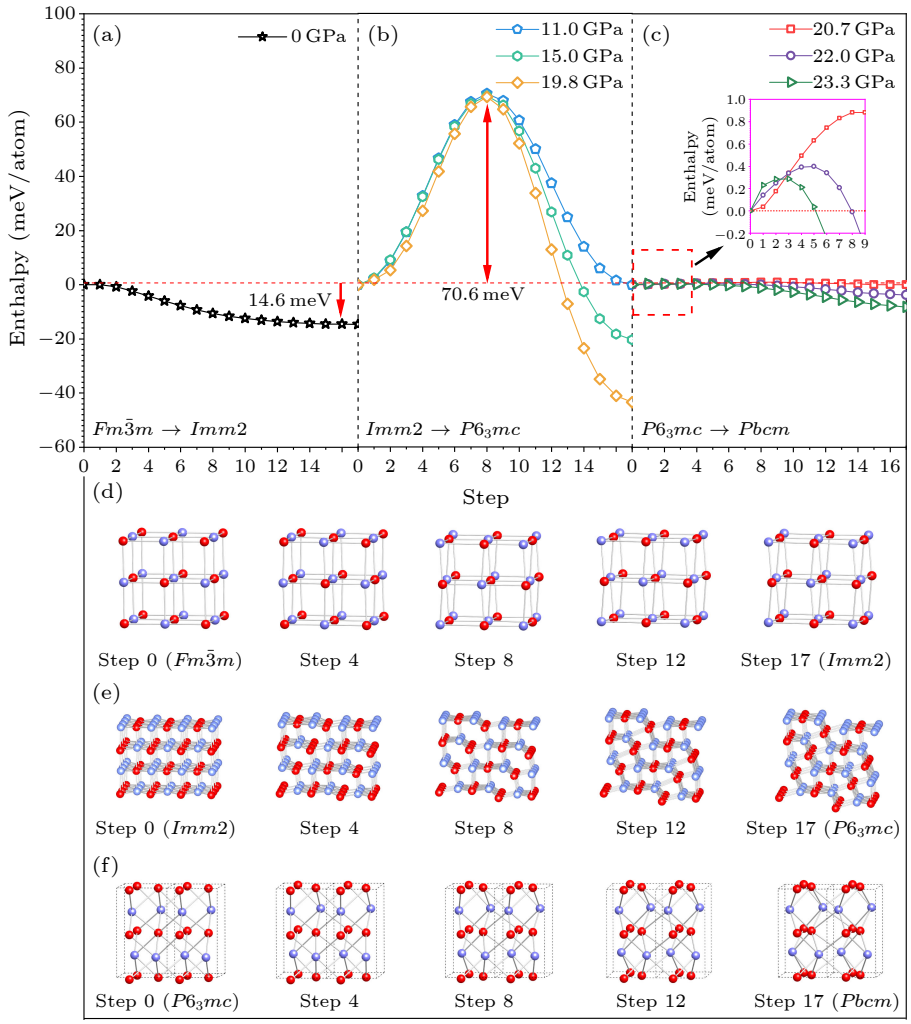

Fig. 6. The G-SSNEB calculations of enthalpy barriers for the structural transitions: (a) the $Fm\bar{3}m$ to the $Imm2$ at 0 GPa; (b) the $Imm2$ to the $P6_3mc$ at 11.0, 15.0, and 19.8 GPa; (c) the $P6_3mc$ to the $Pbcm$ at 20.7, 22.0, and 23.3 GPa. (d)–(f) Minimum enthalpy pathways correspond to each transition.

energetically demanding phase transition. In contrast, the transitions from the $Fm\bar{3}m$ to the $Imm2$ (14.6 meV) and from the $P6_3mc$ to the $Pbcm$ (less than 1.0 meV) exhibit much lower enthalpy barriers, reflecting a simpler and more straightforward phase transition process. This variation in enthalpy barriers highlights the differing complexities and thermodynamic characteristics associated with each phase transition. These results further contribute to our understanding of the phase transition mechanisms in LaN under high pressure, showing that while some transitions are energetically favorable and occur with minimal resistance, others require significant enthalpy input and are more complex in nature. The variation in enthalpy barriers highlights the complexity of high-pressure phase transitions and provides a framework for understanding similar transformations in materials with competing structural phases.

4. Conclusions. In this study, we combined first-principles calculations with high-pressure synchrotron XRD experiments to resolve the long-standing controversy over the phase transition sequence and mechanism of LaN. Our results demonstrate that the $Imm2$ structure exhibits thermodynamic stability at 0 GPa and 0 K, and the low enthalpy barrier between the $Imm2$ and the $Fm\bar{3}m$ phases supports the previously proposed possibility of a temperature-induced phase transition. Experimentally, LaN undergoes the following sequence of high-pressure phase transitions: the $Fm\bar{3}m$ to the $P6_3mc$ to the $Pbcm$, with transition pressures occurring at 19.8 GPa and 23.3 GPa, respectively. The hysteresis in the transition from the $Fm\bar{3}m$ to the $P6_3mc$ is primarily attributed to a significant enthalpy barrier, which hinders the transformation under certain pressure conditions. Our study further elucidates the intricate phase transition behavior of LaN under extreme pressures and offers valuable insights into the underlying mechanisms that govern these transitions. These findings provide a comprehensive understanding of LaN's structural transitions and establish a foundation for studying similar behaviors in other lanthanide mononitrides under high pressure.

Acknowledgements. This work was supported by the Natural Science Foundation of China (Grant Nos. T2325013, 12474004, and 52288102), the National Key Research and Development Program of China (Grant

No. 2021YFA1400503), and the Program for Jilin University Science and Technology Innovative Research Team. Reported calculations utilized computing facilities at the High-performance Computing Center of Jilin University.

References

[1] Lei L, Yi M H, Wang Y B, Hua Y J, Zhang J J, Prasad P N, and Xu S Q 2024 *Nat. Commun.* **15** 1140
[2] Ji Y Q, Wang X H, Li X H, Tang W T, Li X Y, Wang X, Li F F, Li L, and Zhou Q 2024 *Chin. Phys. Lett.* **41** 097402
[3] Li P Y, Bi J C, Zhang S D, Cai R, Su G H, Qi F G, Zhang R Y, Wei Z Y, and Cao Y W 2023 *Chin. Phys. Lett.* **40** 087401
[4] Huang Y N, Ye Z F, Liu D Y, and Qiu H Q 2023 *Chin. Phys. Lett.* **40** 097405
[5] Dolg M and Stoll H 1996 *Phys. Chem. Rare Earths* **22** 607
[6] Guo J, Feng S Y, Tao R, Wang G X, Wang Y, and Liu Z F 2023 *Chin. Phys. B* **32** 127509
[7] Chen W C, Lin C M, Maciejko J, and Chen C C 2021 *Comput. Mater. Sci.* **200** 110779
[8] Zhang Y C, Ding C, Zhang K X, Pakhomova A, Chen S, Ding Y J, Jiang S Q, Huang X L, Sun J, and Cui T 2024 *J. Am. Chem. Soc.* **146** 28174
[9] Shan P F, Wang N N, Zheng X Q, Qiu Q Q, Peng Y Y, and Cheng J G 2023 *Chin. Phys. Lett.* **40** 046101
[10] Li X, Bergara A, Zhang X H, Ding S C, Liu Y, and Yang G C 2024 *Phys. Rev. B* **109** 054522
[11] Liu R, Liu S, Zhang Y, Wang P, and Yao Z 2024 *Chin. Phys. Lett.* **41** 066301
[12] Guo J, Cai S, Wang D, Shu H Y, Yang L X, Wang P Y, Wang W T, Tian H F, Yang H X, Zhou Y Z, Zhao J Y, Han J Y, Li J Q, Wu Q, Ding Y, Yang W G, Xiang T, Mao H K, and Sun L L 2023 *Chin. Phys. Lett.* **40** 097401
[13] Lv R, Tu W Q, Shao D F, Sun Y P, and Lu W J 2023 *Chin. Phys. Lett.* **40** 117401
[14] Wang Y C, Lv J, Zhu L, and Ma Y M 2010 *Phys. Rev. B* **82** 094116
[15] Xia K, Gao H, Liu C, Yuan J N, Sun J, Wang H T, and Xing D Y 2018 *Sci. Bull.* **63** 817
[16] Oganov A R and Glass C W 2006 *J. Chem. Phys.* **124** 244704
[17] Pickard C J and Needs R 2011 *J. Phys. Condens. Matter* **23** 053201
[18] Zhou D, Li Q, Zheng W T, Ma Y, and Chen C F 2017 *Phys. Chem. Chem. Phys.* **19** 4560
[19] Zhou D, Li Q, Ma Y M, Cui Q L, and Chen C F 2013 *J. Phys. Chem. C* **117** 5352
[20] Kong J, Su L, Cui H X, Ding H R, Hou J Y, Chi C X, Liu S Y, Zhou X F, Wang H T, and Dong X 2024 *Chin. Phys. Lett.* **41** 107101
[21] Chen R T, Zhang J, Wang Z L, Lu K, Peng Y, Zhao J F, Feng S M, and Jin C C 2024 *Chin. Phys. Lett.* **41** 126102
[22] Niu J J, Lu Z Y, Nan S, Wu X, Qin S, Liu Y X, and Li W X 2023 *J. Am. Ceram. Soc.* **106** 6292
[23] Li Q, Ma Y M, Oganov A R, Wang H B, Wang H, Xu Y, Cui T, Mao H K, and Zou G T 2009 *Phys. Rev. Lett.* **102** 175506
[24] Young R and Ziegler W 1952 *J. Am. Chem. Soc.* **74** 5251
[25] Gökoğlu G, and Erkişi A 2008 *Solid State Commun.* **147** 221
[26] Miao J Y, Sun W G, Peng F, and Lu C 2024 *Eur. Phys. J. Plus* **39** 1025
[27] Vaitheeswaran G, Kanchana V, and Rajagopalan M 2002 *Solid State Commun.* **124** 97
[28] Ciftci Y, Colakoglu K, Deligoz E, and Ozisik H 2008 *Mater. Chem. Phys.* **108** 120
[29] Ghezali M, Amrani B, Cherchab Y, and Sekkal N 2008 *Mater. Chem. Phys.* **112** 774
[30] Yang X C, Liu F, Luo X Y, Lin H Y, and Xiao J P 2013 *Appl. Mech. Mater.* **331** 563
[31] Mukherjee D, Sahoo B, Joshi K, and Gupta S C 2013 *High Press. Res.* **33** 563
[32] Schneider S B, Baumann D, Salamat A, and Schnick W 2012 *J. Appl. Phys.* **111** 093503
[33] Ding C, Yuan J N, Cogollo-Olivo B H, Wang Y L, Wang X M, and Sun J 2023 *Sci. China Phys. Mech. Astron.* **66** 228211
[34] Mao H K, Xu J, and Bell P M 1986 *J Geophys. Res. Solid Earth* **91** 4673
[35] Ruoff A L, Luo H, Vanderborgh C, Xia H, Brister K, and Arnold V 1993 *Rev. Sci. Instrum.* **64** 3462
[36] Hammersley A P, Svensson S O, Hanfland M, Fitch A N, and Hau-sermann D 1996 *High Press. Res.* **14** 235
[37] Larson A C 1990 Report LAUR 86-748 (Los Alamos National Laboratory) **121**
[38] Toby B H 2001 *J. Appl. Crystallogr* **34** 210
[39] Kresse G and Furthmüller J 1996 *Comput. Mater. Sci.* **6** 15
[40] Kresse G, and Furthmüller J 1996 *Phys. Rev. B* **54** 11169
[41] Perdew J P, Burke K, and Ernzerhof M 1996 *Phys. Rev. Lett.* **77** 3865
[42] Wang Y C, Liu H Y, Lv J, Zhu L, Wang H, and Ma Y M 2011 *Nat. Commun.* **2** 563
[43] Wang F C, Ye Q J, Zhu Y C, and Li X Z 2024 *Phys. Rev. Lett.* **132** 086101
[44] Sheppard D, Xiao P H, Chemelewski W, Johnson D D, and Henkel-man G 2012 *J. Chem. Phys.* **136** 074103
[45] Sheppard D and Henkelman G 2011 *J. Comput. Chem.* **32** 1769
[46] Parlinski K, Li Z, and Kawazoe Y 1997 *Phys. Rev. Lett.* **78** 4063
[47] Hellman O, Steneteg P, Abrikosov I A, and Simak S I 2013 *Phys. Rev. B* **87** 104111
[48] Shao S, Lv J, Li X, Li L, Liu P, Liu Z D, Chen C F, Wang Y C, and Ma Y M 2024 *Phys. Rev. Lett.* **133** 214101
[49] Wang Y Z, Cui X H, Liu J, Jing Q, Duan H M, and Cao H B 2024 *Chin. Phys. B* **33** 016109
[50] Lu C W, Yang K, Cui W W, Hao J, Shi J M, and Li Y W 2024 *Phys. Rev. B* **110** 024111
[51] Shen J Y, Duan Q Z, Miao J Y, He S, He K H, Dai W, and Lu C 2023 *Chin. Phys. B* **32** 096302
[52] Gong W G, Xu R, Shao X C, Li Q, and Chen C F 2021 *Phys. Rev. Mater.* **5** 123606
[53] Liu J Y, Liu A L, Wang Y J, Gao L L, Luo X Y, and Zhang M 2025 *Chin. Phys. B* **34** 046201
[54] He X L, Zhao W B, Xie Y, Hermann A, Hemley R J, Liu H Y, and Ma Y M 2024 *Proc. Natl. Acad. Sci.* **121** e2401840121
[55] Wang M H, Wang Z X, Wang G T, Song H L, Fu Y H, Li L, and Cui Z H 2024 *Nano Lett.* **24** 11831
[56] Chakraborty T, Rogal J, and Drautz R 2016 *Phys. Rev. B* **94** 224104